Improving the absolute accuracy of the gravitational wave detectors by combining the photon pressure and gravity field calibrators

Yuki Inoue,[1, 2] Sadakazu Haino,[1, 2] Nobuyuki Kanda,[3] Yujiro Ogawa,[2, 4] Toshikazu Suzuki,[2, 5, 6] Takayuki Tomaru,[2, 4, 5, 6] Takahiro Yamanmoto,[7] and Takaaki Yokozawa[7]

[1]*Institute of Physics, Academia Sinica, Taipei 11529, Taiwan*
[2]*High Energy Accelerator Research Organization (KEK), Ibaraki 305-0801, Japan*
[3]*Department of Physics, Graduate School of Science, Osaka City University, Osaka 558-8585, Japan*
[4]*SOKENDAI(The Graduate University for Advanced Studies),*
Hayama, Miura District, Kanagawa 240-0115, Japan
[5]*Kavli Institute for the Physics and Mathematics of the Universe (Kavli IPMU),*
The University of Tokyo, Chiba 277-8568, Japan
[6]*Institute for Cosmic Ray Research, The University of Tokyo, Chiba 277-8582, Japan*
[7]*Institute for Cosmic Ray Research, The University of Tokyo, Gifu 506-1205, Japan*

The absolute accuracy of the estimated parameters of gravitational wave sources will be fundamentally limited by the calibration uncertainties of the detectors in upcoming observation runs with the increased number of source statistics. Photon calibrators have so far been the primary tools for absolute calibration of test-mass displacement, relying on measurement of the photon pressure. The current technological limit of the absolute calibration uncertainty for gravitational-wave amplitudes is limited to a few percent, due to the uncertainty in the laser power-standard maintained by the metrology institutes. To reduce this uncertainty, this article proposes a novel calibration method that combines a photon calibrator and a gravity field calibrator. The gravity field calibrator achieves modulation of the displacement of the test mass by generating a gravity gradient. In previous studies, uncertainty in the distance between the test mass and the gravity field calibrator has proven a serious source of systematic error. To suppress this uncertainty, we propose a novel method that uses a combination of quadrupole and hexapole mass distributions in the gravity field calibrator. We estimate the absolute uncertainty associated with method to be as low as 0.17 %, which is ten times less than that of previous methods.

I. INTRODUCTION

The discovery of gravitational waves (GW) has given us the new probe for observing the universe [1]. The typical strain sensitivity, h, of second generation interferometric detectors, such as Advanced LIGO [2], Advanced Virgo [3], and KAGRA [4, 5], is around $10^{-23}/\sqrt{\text{Hz}}$ at 100 Hz.

In GW150914 event data analysis, it has been shown that the calibration errors give significant impact on the sky localization accuracy. The 90 % sky confidence region gets larger from 150 deg^2 to 610 deg^2 by introducing the calibration uncertainties of 10 % in amplitude and 10 degrees phase [6], and eventually got smaller to 230 deg^2 with the improved calibration uncertainties [7, 8]. Using GW signals from compact binary coalescences events, researchers can derive several parameters of the source objects such as masses, spins, luminosity distance, orbital inclination and the sky location. The precision of these derived parameters is limited by the calibration accuracy. As the number of detected sources increases and events with higher signal-to-noise ratio (SNR) are detected, calibration uncertainty will become the dominant source of errors when extracting physical informations from the signals. Testing general relativity has been demonstrated with the GW events from binary black hole mergers [9]. In most of the analysis, the effect of calibration uncertainties on the detection and parameter estimation of GW events have focused on placing constrains on the calibration accuracy by modeling the calibration errors as smooth and random frequency-dependent fluctuations. By a semi-analytic approach to explicitly relate systematic errors in calibration parameters to the GW signal parameters, it has been shown that for events with SNR 20, calibration accuracy of a few percent is required for certain parameters such as optical gain and actuation strength in order to achieve noise-limited systematics [10]. Upper limits and observations of continuous GW waves such as rapidly rotating neutron stars and stochastic background of unresolvable sources depend on calibration uncertainties. The associated uncertainties on the upper limits of continuous waves amount to 20 % by including 10 % amplitude calibration uncertainty [11, 12]. The suppression of the calibration error also improve burst GW reconstruction. Especially, the precise correction of the frequency dependence will remove the biases on arrival time and polarization components. These parameters affects on estimations for a source direction and rotational axis of SN core, respectively. In the idea to estimate a mass of an isolated neutron star using gravitational waves [13, 14], it must determine the phase difference precisely between once and twice spin frequency modes. For many known pulsar cases, these frequencies are around the unity gain frequency where the transfer function phase changes steeply. Also, since the continuous wave measurement would use a long-duration data sets as a order of years, the robustness and stableness of calibrations is essentially important. In particular, the

uncertainty in the absolute amplitude of the GW signal propagates directly into the estimation of the distance to the sources. The rate that compact binary system coalescences in the universe if drawn from detected events. The SNR by the searches are quadratically sensitive to the calibration errors since they are maximized over arrival time, waveform phase, and the template banks. The amplitude calibration uncertainty of 10 % and the derived uncertainty of the luminosity distances of the sources corresponds to an approximately 30 % uncertainty in volume and will dominate over the statistical uncertainty [15]. The detection of a GW signal from the GW170817 Binary Neutron Star (BNS) system, along with a concurrent electromagnetic (EM) signal, began a new era of multimessenger astronomy [16]. These observations allow us to use GW170817 as a standard siren [17–20] with witch we can determine the absolute luminosity distance to the source directly from the GW signals. Assuming an event rate of 3000 $\mathrm{Gpc}^{-3}\mathrm{yr}^{-1}$ which is consistent with the 90 % confidence interval for GW170817 [16], we expect that GW signals will be detected from about 50 BNS standard sirens dureing the next few observing runs. These observations can constrain the Hubble constant (H_0) to 2 % error or less [21], and eventually resolve the 3-σ tension in H_0 measurements between Cephied-SN distance ladder [22] and CMB data when assuming the ΛCDM model. [23] Systematic errors in the calibration of the absolute GW signal amplitude must be suppressed less than 1 % to achieve higher-precision H_0 measurements using GW standard sirens.

Laser interferometers measure change in distance along the two interferometer arms. Fluctuations in the degree of freedom of the differential arm length (DARM) are suppressed by a DARM control loop. The reconstruction of the DARM fluctuation at the observation frequency is affected by the GWs. The gravitational waveform can be reconstructed from the calibrated error and control signals of this DARM loop. To calibrate these signals, accurate physical models of the actuator and sensing function are essential. These models require measurements of the transfer function and monitoring of the time dependency of the transfer function using continuous sine waves (calibration lines). The residual of the time-dependent model corresponds to the uncertainty of the observaton.

To reduce the systematic uncertainty in the calibration, we need to inject well-parameterized calibration lines for the photon calibrator (Pcal) or other calibration sources for monitoring the time variation of the interferometer responce. The Pcal was developed by the Glasgow and GEO600 reserch groups [24, 25], followed by Advanced LIGO which particularly improved Pcals for calibrating the time-dependent response of interferometers [3, 26–28]. However, Pcal still face a challenges in finding of the absolute amplitude calibration because of the uncertainty in the laser power standards published by different national metrology institutes [29]. The absolute power between these institutes vary by a few % [30].

Gravity field calibrator (Gcal) is one of the most promising candidates to be able to solve the uncertainty problem of the absolute laser amplitude calibrations. The technology has been developed and tested by Forward and Miller [31], Weber [32, 33], University of Tokyo [34–38] and Rome university group [39, 40]. Related techniques using Gcal are discussed in Matone $et.$ $al.$ and Raffai $et.$ $al.$ [41, 42]. The device can modulate a test mass using a gravity gradient generated by a rotor that depending on the masses, distance, frequency, radius, and the gravity constant.

This paper proposes new method for achieving subpercent uncertainty in the absolute amplitude calibration of the GW detectors. The method combines Pcal and Gcal. Section II explains the methods used for Pcal. In section III, we discuss the principle of a multipole moment of gravity and how it is modulated to derive a calibration signal. We demonstrate how to calibrate absolute displacement using two calibrators in concert in section IV, and in section V, we discuss the contributions of the systematic error and estimate the current technological limits on the gravitational wave observation from typical physical assumptions.

II. PHOTON CALIBRATOR

Pcal exploit how the photon radiation pressure from power-modulated laser beams reflects from a test mass. The periodic photon recoil applies a periodic force to test mass [26]. Advanced LIGO, Advanced Virgo and KAGRA employ Pcals for the calibration of the interferometer response [3, 43, 44]. All of them use laser of the same wave length, 1047 nm, to actuate the test mass. The test mass displacement is described as

$$x = \frac{2P\cos\theta}{c}s(\omega)\left(1 + \frac{M}{I}\vec{a}\cdot\vec{b}\right), \qquad (1)$$

where P is the absolute laser power, θ is the incident angle of the Pcal laser, M is the mass of test mass, ω is the angular frequency of the laser power modulation, and $\vec{a}$ and $\vec{b}$ are the position vectors of the Pcal laser beams. A schematic view of device is shown in Fig. 1. $I = Mh^2/12 + Mr^2/4$ is the moment of inertia, where h and r are the thickness and radius of the test mass, respectively. $s(\omega)$ is the transfer function between force and displacement. We can regard the value of $s(\omega)$ as $1/(M\omega^2)$ at the frequency above 20 Hz, as the test mass behaves as a free mass in this regime.

The amplitude of the laser power noise is stabilized to be less than the design sensitivity. As shown in Fig. 1, the power stabilized laser is mounted on the transmitter module. The power of the photo detector responses at the transmitter module, V_{TxPD}, and receiver module, V_{RxPD} are monitored for differences. The largest relative uncertainty of photon calibrator is that of laser power. Advanced LIGO and KAGRA use a working standard to cross-calibrate the relative interferometer responces. The
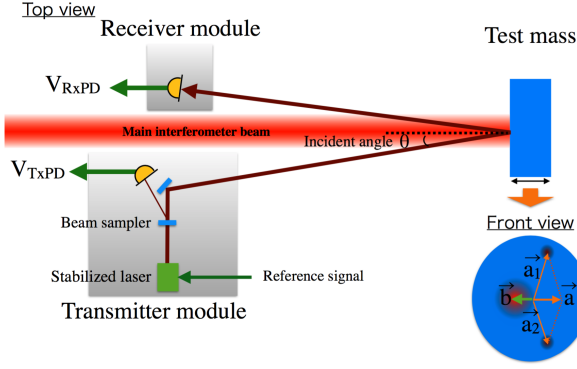
FIG. 1. Schematic view of photon calibrator. The stabilized laser is placed on the transmitter module. The signal injected to the test mass is monitored through the difference in photo detector responce power between the transmitter module and receiver module,V_{TxPD} and V_{RxPD}. The geometrical factor is characterized in term of the position vectors of the photon calibrator beams, $\vec{a} = \vec{a_1} + \vec{a_2}$, and the main beam, $\vec{b}$.

TABLE I. Specification summary of Advanced LIGO, Advanced Virgo and KAGRA photon calibrator.

	KAGRA	Advanced LIGO	Advanced Virgo
Mirror material	Sapphire	Silica	Silica
Mirror mass	23 kg	40 kg	40 kg
Mirror diameter	220 mm	340 mm	350 mm
Mirror thickness	150 mm	200 mm	200 mm
Distance from Pcal to test mass	36 m	8 m	1.5 m
Pcal laser power	20 W	2 W	3 W
Pcal laser frequency	1047 nm	1047 nm	1047 nm
Incident angle	0.72 deg	8.75 deg	30 deg

relative uncertainty of each calibrator is 0.51 % [26]. The second largest relative uncertainty is the optical efficiency of the optical path in the calibrator. We calibrate the injected power from the exterior of the vacuum chamber. Therefore, we need to consider the difference in optical efficiency due to the transmittance of the vacuum window and the reflectance of the mirrors. The measured uncertainty of the optical efficiency in the Advanced LIGO is 0.37 %. For absolute calibration, the photo detector, following the so called gold standard, is calibrated using the laser power standard maintained by the National Institute of Standards and Technology (NIST) in Boulder, CO [45] in the U.S. The working standard responces for Hanford, Livingston and KAGRA GW detectors are calibrated to this gold standard. However, a comparison of the accuracies of the absolute laser power standards maintained by each national standard institute shows a few % uncertainty [29]. This uncertainty leads to the serious systematic error in the distance calibrations propagated from the uncertainty of the absolute calibration.
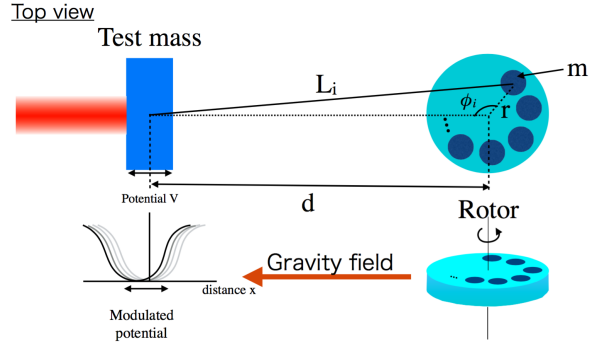

FIG. 2. Schematic of Gcal. The rotor is placed at the same height as the test mass and at a distance of d. Multipole masses spinning around the rotor generate a varying gravitational potential at the position of test mass.

III. GRAVITY FIELD CALIBRATOR

To address this problem of uncertainty in the the absolute calibration, we propose a new calibration method that combines Pcal and Gcal. The Gcal generates a dynamic gravity field by rotating the multipole masses with a rotor placed in a vacuum chamber that isolates acoustic noise. To monitor the frequency of this rotation, an encoder with a 16-bit analog to digital converter is included. Next, we calculate the displacement of the test mass in the dynamic gravity field generated by a multipole moment with N masses. The calculation assumes a free-mass of a test mass and a set of masses mounted on a disk as shown in Fig 2. The rotating the masses m are arranged around the rotor at radius, r. The distance between the center of this rotor and the test mass mirror is assumed d. We rotate the disk rotates at the angular frequency $\omega_{\rm rot} = 2\pi f_{\rm rot}$.

We estimate the equation of motion of the test mass as it is moved by the dynamic gravity field. First, we calculate the distance between the test mass and the N pieces of masses arranged around the rotor. The distance between i-th mass and the center of test mass is written as

$$L_i = d\sqrt{1 + \left(\frac{r}{d}\right)^2 - 2\left(\frac{r}{d}\right)\cos\phi_i}, \qquad (2)$$

where the angle of the i-th mass is assumed to be $\phi_i = \omega_{\rm rot}t + 2\pi i/N$. The gravitational potential at the center of test mass can be described as

$$V = \Sigma_{i=0}^{N}V_i, \qquad (3)$$
$$= -GMm\Sigma_{i=0}^{N}L_i^{-1}, \qquad (4)$$
$$= -\frac{GMm}{d}\Sigma_{i=0}^{N}\Sigma_{n=0}^{\infty}\left(\frac{r}{d}\right)^n P_n\left(\cos\left(\omega_{\rm rot}t+\frac{2\pi i}{N}\right)\right), (5)$$

where P_n is the Legendre polynomial, and V_i is the potential of a mass. The equation of motion of the test
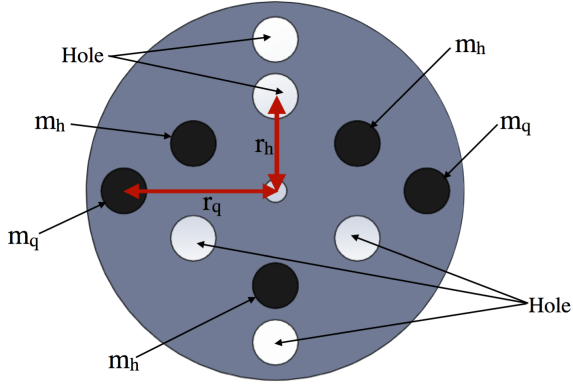
FIG. 3. Configuration of the rotor with quadrupole and hexapole mass distributions. m_q and m_h are the masses of quadrupole and hexapole masses. r_q and r_h are the radii of the quadrupole and arrangements hexapole.

mass is

$$Ma = \left| \frac{\partial V}{\partial d} \right| = \frac{GMm}{d^2} \Sigma_{i=0}^{N} \Sigma_{n=0}^{\infty} (n+1) \left(\frac{r}{d} \right)^n \times P_n \left(\cos \left(\omega_{rot} t + \frac{2\pi i}{N} \right) \right), \tag{6}$$

where a is the acceleration of the test mass.

We arrange the masses around the rotor in a superposition of quadrupole and hexapole arrangements, as shown in Fig. 3. A hole is placed between each mass. These holes is effectively double the magnitude of the gravity gradient. Therefore, the equation of motion of the test mass is

$$Ma = \left| \frac{\partial V}{\partial d} \right| = \frac{2GMm}{d^2} \Sigma_{i=0}^{N} \Sigma_{n=0}^{\infty} (n+1) \left(\frac{r}{d} \right)^n \times P_n \left(\cos \left(\omega_{rot} t + \frac{2\pi i}{N} \right) \right). \tag{7}$$

Next, we will calculate the displacements of the quadrupole and hexapole rotor masses in sections III A and III B.

A. Displacement of test mass driven by quadrupole mass distribution

We calculate the displacement of the quadrupole mass distribution with two pieces and two holes so $N = 2$. The masses and radii of the quadrupole arrangement are m_q and r_q. The equation of motion for the test mass is

$$Ma = \frac{2GMm_q}{d^2} \Sigma_{n=0}^{\infty} (n+1) \left(\frac{r_q}{d} \right)^n \times \Sigma_{i=0}^{1} P_n \left(\cos \left(\omega_{rot} t + \pi i \right) \right). \tag{8}$$

If we assume $r \ll d$, the displacement of the time-dependent lower harmonics can be written as

$$x = \Sigma_{k=1}^{\infty} x_{kf} \cos(k\omega_{rot} t) \sim x_{2f} \cos(2\omega_{rot} t) = x_{2f} \cos \omega t, \tag{9}$$

where k is the number of the harmonics. The amplitude of the 2-f rotation is then

$$x_{2f} = 9 \frac{GMm_q r_q^2}{d^4} s(\omega). \tag{10}$$

B. Displacement of test mass driven by hexapole mass distribution

We also calculate the displacement of the hexapole mass distribution with three holes as $N = 3$. The masses and radii of the hexapole distribution are m_h and r_h. The equation of motion of test mass driven by this arrangement alone is

$$Ma = \frac{2GMm_h}{d^2} \Sigma_{n=0}^{\infty} (n+1) \left(\frac{r_h}{d} \right)^n \times \Sigma_{i=0}^{2} P_n \left(\cos \left(\omega_{rot} t + \frac{2\pi i}{3} \right) \right). \tag{11}$$

If we assume $r \ll d$, the displacement of the time-dependent lower harmonics can be written as

$$x = \Sigma_{k=1}^{\infty} x_{kf} \cos(k\omega_{rot} t) \sim x_{3f} \cos(3\omega_{rot} t) = x_{3f} \cos \omega t, \tag{12}$$

where amplitude of 3-f is described as

$$x_{3f} = 15 \frac{GMm_h r_h^3}{d^5} s(\omega). \tag{13}$$

IV. ABSOLUTE POWER CALIBRATION WITH BOTH PHOTON AND GRAVITY FIELD CALIBRATOR

This section discusses how to combine the calibration signals from Pcal and Gcal to allow absolute laser power calibration using an interferometer. Figure 4 diagrams the combined calibration system. First, the test mass is driven by the Gcal. The x_{2f} and x_{3f} signals are measured from the response of the interferometer. Second, this interferometer signal is sent to the excitation port of the Pcal. This signal acts as a reference signal for feedback control, as shown in Fig. 4. The Pcal then cancels out the displacement modulated by the Gcal. Third, the voltage responses of the transmitter and the receiver module photodetectors are measured. The output signal of the transmitter module, V_{TxPD} and receiver module, V_{RxPD} should correspond to the displacement caused by the Gcal. By using Eq (1),(10), and (13), the modulated signal powers are

$$P_{2f} = \frac{9}{2} \frac{Gcm_q M r_q^2}{d^4 cos\theta} \frac{1}{1 + \frac{M}{I} \vec{a} \cdot \vec{b}}, \tag{14}$$

$$P_{3f} = \frac{15}{2} \frac{Gcm_h M r_h^3}{d^5 cos\theta} \frac{1}{1 + \frac{M}{I} \vec{a} \cdot \vec{b}}. \tag{15}$$
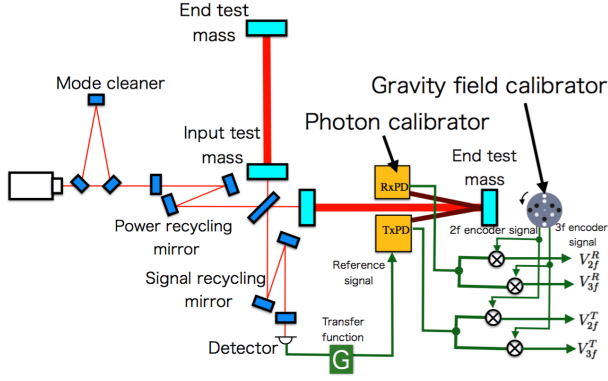
FIG. 4. Test apparatus for the absolute calibration. The Gcal is placed behind the test mass. The frequency of the Gcal is monitored with the encoder output. The error signal for the differential arm length of the interferometer is sent to the reference port of the photon calibrator for canceling the modulation of the dynamic gravity field with feedback with transfer function G. Output signals from the photon calibrator are synchronized with the forces driven by the Gcal. The output signals are demodulated with 2-f and 3-f signals monitored by the encoder.

Fourth, we demodulate the signal of the transmitter and receiver modules using the measured encoder signal from the Gcal. The demodulated signals are

$$V_{2f}^{T} = \rho_T P_{2f}, \qquad (16)$$
$$V_{2f}^{R} = \rho_R P_{2f}, \qquad (17)$$
$$V_{3f}^{T} = \rho_T P_{3f}, \qquad (18)$$
$$V_{3f}^{R} = \rho_R P_{3f}, \qquad (19)$$

where ρ_T and ρ_R are the transfer functions from power to the photo detector output voltages at the transmitter and receiver modules. Therefore, we can measure the distance from the ratio of responses of the 2-f and 3-f components:

$$d = \frac{5}{3}\frac{V_{2f}^{T}}{V_{3f}^{T}}\frac{m_h}{m_q}\frac{r_h^3}{r_q^2} = \frac{5}{3}\frac{V_{2f}^{R}}{V_{3f}^{R}}\frac{m_h}{m_q}\frac{r_h^3}{r_q^2}. \qquad (20)$$

Finally, we calculate the displacement formula for the Pcal calibrated by Gcal. We substitute the Eq. (10) to Eq. (1) to obtain the following equation for displacement:

$$x = \frac{2P\cos\theta}{c}s(\omega)\left(1 + \frac{M}{I}\vec{a}\cdot\vec{b}\right), \qquad (21)$$

$$= 9\frac{Gm_q M r_q^2}{d^4}\frac{P}{P_{2f}}s(\omega), \qquad (22)$$

$$= \frac{729}{625}\frac{GMm_q^5 r_q^{10}}{m_h^4 r_h^{12}}\frac{V_{3f}^{R4}}{V_{2f}^{R5}}V_{in}s(\omega), \qquad (23)$$

where we assumed that $P(\omega) = \rho_R V_{in}$, and V_{in} is the amplitude of the input voltage. The factor $(GMm_q^5 r_q^{10})/(m_h^4 r_h^{12})$ can be measured before the calibration. V_{3f}^{R}/V_{2f}^{R} is measured during the calibration of

the Gcal and Pcal. The interval of the calibration signals between the Pcal and Gcal depend on the stability of the photon calibrator laser power. The Advanced LIGO experiment calibrates the absolute laser power using the working standard monthly. Therefore, The Gcal should be run monthly or more frequently. The present method reconstructs the Pcal signal from Gcal signals. Therefore, the Gcal does not need to be operated during observation runs. During operation, the Gcal would contaminate the noise floor by adding acoustic and/or vibration noise. However, we can minimize this noise effect by controlling the rotation frequency. The above analysis has not considered to the noise added by the Gcal during observation runs, as we only propose that the Gcal be used to calibrate the absolute displacement before the observations. The demodulation technique allows us to reduce the systematic error introduced by rotation . When the modulation of Gcal is canceled using Pcal, the transfer functions of the Gcal and Pcal are also canceled. Therefore, the estimated displacement of the test mass does not depend on the frequency of the rotation.

V. ESTIMATION OF UNCERTAINTY

In this section, we evaluate the accuracy of the estimated displacement, and discuss the effects on systematic error by changing the operating frequency and distance. After that, we discuss the uncertainty in the displacement of the mirror. The following discussion assumes the basic parameters of the KAGRA experiment listed in Table I, and the parameters of the Gcal as listed in Table II.

A. Systematic error of higher order terms

To achieve the precision less than 1 %, we need to consider the effect of higer-order Legendre polynomials at the position of the test mass. This is because higher-order polynomials also affect the 2-f and 3-f components. The n-th order Legendre polynomial is calculated with Eq.(7). The effect of higher-order factors is mitigated by the factor $(r/d)^n$. Tables III and IV show the calculated dis-

TABLE II. Assumed parameters. G is gravity constant [46]. θ is incident angle of the Pcal beams. M is mass of test mass. $1 + \frac{I}{M}\vec{a}\cdot\vec{b}$ is geometrical factor.

	Value	Relative uncertainty
G	6.67408×10^{-11} m^{3}kg^{-1}sec^{-2}	0.0047 %
$\cos\theta$	1.000	0.07 %
M	22.89 kg	0.02 %
m_q	4.485 kg	0.004 %
m_h	4.485 kg	0.004 %
r_q	0.200 m	0.010 %
r_h	0.125 m	0.016 %
$1 + \frac{I}{M}\vec{a}\cdot\vec{b}$	1	0.3 %

TABLE III. Calculated quadrupole ($N = 2$) displacement. n is the order of the Legendre polynomial, where $\omega = n\omega_{\rm rot}$.

	n=1	n=2	n=3	n=4	n=5	n=6	n=7
1-f	0	0	0	0	0	0	0
2-f	0	$9\frac{Gmr^2}{d^4\omega^2}$	0	$\frac{25}{4}\frac{Gmr^4}{d^6\omega^2}$	0	$\frac{735}{128}\frac{Gmr^6}{d^8\omega^2}$	0
3-f	0	0	0	0	0	0	0
4-f	0	0	0	$\frac{175}{16}\frac{Gmr^4}{d^6\omega^2}$	0	$\frac{273}{32}\frac{Gmr^6}{d^8\omega^2}$	0
5-f	0	0	0	0	0	0	0
6-f	0	0	0	0	0	$\frac{1617}{128}\frac{Gmr^6}{d^8\omega^2}$	0

TABLE IV. Calculated hexapole ($N = 3$) displacement. n is the order of the Legendre polynomial, where $\omega = n\omega_{\rm rot}$.

	n=1	n=2	n=3	n=4	n=5	n=6	n=7
1-f	0	0	0	0	0	0	0
2-f	0	0	0	0	0	0	0
3-f	0	0	$15\frac{Gmr^3}{d^5\omega^2}$	0	$\frac{315}{32}\frac{Gmr^5}{d^7\omega^2}$	0	$\frac{567}{64}\frac{Gmr^7}{d^9\omega^2}$
4-f	0	0	0	0	0	0	0
5-f	0	0	0	0	0	0	0
6-f	0	0	0	0	0	$\frac{4851}{256}\frac{Gmr^6}{d^8\omega^2}$	0

placements of the higher order terms. To investigate the higher order effects, we compare the estimated test mass displacement between the Legendre polynomial approximation and numerical calculations of $\frac{\partial V}{\partial d}$ and Eq.(5). The ratio of two calculations of the test mass displacement is shown in Figs. 5 and 6 for the quadrupole ($N = 2$) and hexapole ($N = 3$) components, respectively, as a function of the distance, d. The results show that the effect of higher-order of polynomials is less than that of systematic error. The mirror therefore needs to be placed at least 2 m away from the rotating mass. Then the sum of the first and second order equations can be used to suppress the systematic error well below 1 % as shown in Figs. 5 and 6. If we place the Gcal near the KAGRA end test mass, the distance of 2 m is reasonable. The rotor could be mounted outside of the vacuum chamber. In the following calculations, we assume $d = 2$ m for the simplification of the discussion. The analytical calculation of the displacement of the test mass in Eq.(7) assumes that the rotor masses and the test mass can be approximated as point masses. We compared the results of this analytical calculation with the numerical integral of the displacements generated by the actual dimensions of the rotor with the parameters shown in Table II, and confirmed that the analytical formula is sufficiently at $d = 2$ m.

B. Systematic error of the transfer function

The Gcal modulates the test mass mirror with gravitational potential gradient. However, this gradient also actuates the masses of suspension system as shown in Fig. 7. We simulated the transfer function with the assumption of the cryogenic suspension system installed in
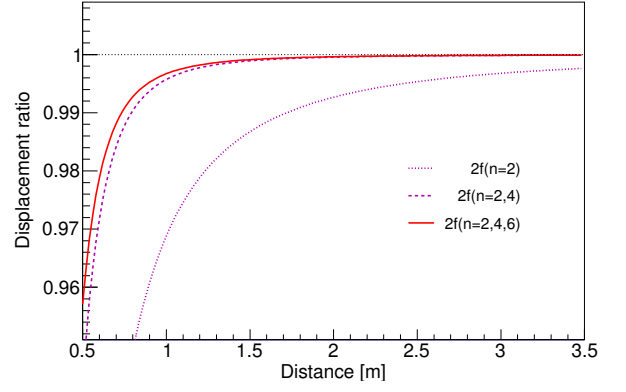

FIG. 5. Ratio of Legendre polynomial approximations with the numerical calculations of $\frac{\partial V}{\partial d}$ and Eq.(5) on the test mass displacement for the quadrupole ($N = 2$) component as a function of the distance. Dotted, dashed and solid lines correspond to first-order only, second-orders, and third-order approximations, respectively. The analytical results are listed in Table III. To achieve precision less than 1 %, the higher-order terms need to be included.
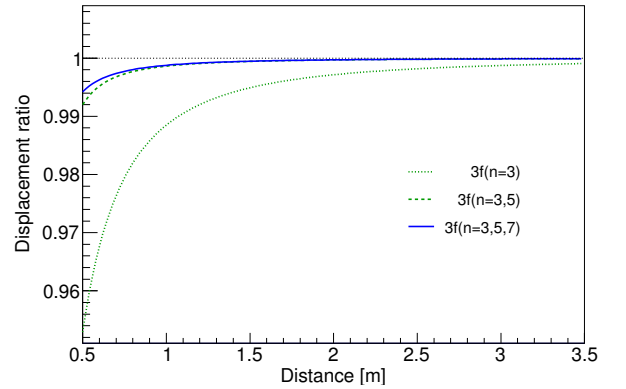

FIG. 6. Ratio of the Legendre polynomial approximation to the numerical calculations of $\frac{\partial V}{\partial d}$ and Eq.(5) on the test mass displacement for the hexapole distribution ($N = 3$) component as a function of distance. The dotted, dashed and solid lines correspond to the first-order only, second-orders, and third-orders, respectively. The analytical result is listed in Table IV. To achieve the precision less than 1 %, the higher-order terms need to be included..

KAGRA [47].The transfer function was calculated using the rigid-body suspension simulation code, called SUM-CON [48]. We estimated the total displacement by superimposing the displacements driven by both mass distributions. Figure 8 shows the displacement ratio between the motion signal and the free-mass motion as a function of frequency. The simulation result is in good agreement with the free-mass motion at this frequencies larger than 20 Hz. The low frequency structures correspond to the resonant peak of the suspension system. Therefore,
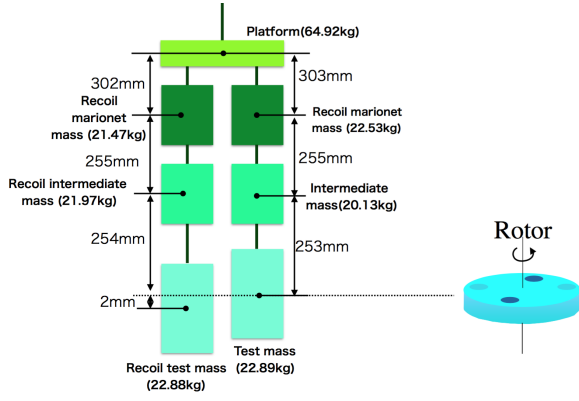
FIG. 7. Schematic of the suspension system. The parameters of the heights and masses are marked with their assumed values.
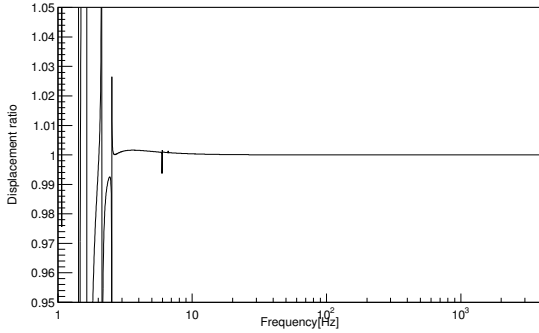

FIG. 8. Displacement ratio of the transfer function for mult-pendulums by changing modulation frequency. The relations of the modulation frequency, f, modulation angular frequency, ω, and rotation angular frequency $\omega_{\rm rot}$ are described as $n\omega_{\rm rot} = \omega = 2\pi f$.

we can neglect this intermediate-mass effect and regard as motion at frequency over 20 Hz as free-mass motion. Therefore, we need to operate the rotor at speeds larger than 20 Hz to achieve error less than 0.1 %. We assumed the rotation frequency to be 16 Hz, which corresponds to 32 Hz and 48 Hz for the effective frequency of the 2-f and 3-f components. This assumption applies to the discussion in the next section.

C. Uncertainty of displacement and laser power

In this section, we estimate the typical displacement based on the result in Table. II. We neglect Legendre polynomials of degree higher than twwo in the following discussion to simplify the discussion, though they are relevant in the calculations. The estimated 2-f and 3-f

displacements are described as

$$
x_{2\rm f}^{\rm rms} = 1.18 \times 10^{-16}[\rm m] \times \left(\frac{G}{6.67408 \times 10^{-11}[\rm m^3 kg^{-1} sec^{-2}]} \right)
$$
$$
\times \left(\frac{m_{\rm q}}{4.485[\rm kg]} \right) \times \left(\frac{r_{\rm q}}{0.200[\rm m]} \right)^2 \times \left(\frac{2[\rm m]}{d} \right)^4 \times \left(\frac{2\pi \times 32[\rm Hz]}{\omega} \right)^2 \quad (24)
$$
$$
x_{3\rm f}^{\rm rms} = 2.13 \times 10^{-18}[\rm m] \times \left(\frac{G}{6.6742 \times 10^{-11}[\rm m^3 kg^{-1} sec^{-2}]} \right)
$$
$$
\times \left(\frac{m_{\rm h}}{4.485[\rm kg]} \right) \times \left(\frac{r_{\rm h}}{0.125[\rm m]} \right)^3 \times \left(\frac{2[\rm m]}{d} \right)^5 \times \left(\frac{2\pi \times 48[\rm Hz]}{\omega} \right)^2 \quad (25)
$$

We define the signal-to-noise ratio (SNR) in the term of the ratio of RMS displacement of the design noise spectrum density for the interferometer of KAGRA at 32 Hz for 2-f and 48 Hz for 3-f. Using this result, we estimate the SNR of the peaks.

$$
SNR_{2\rm f} = 392 \times \left(\frac{3.0 \times 10^{-19}[\rm m/\sqrt{Hz}]}{n_{32\rm Hz}} \right) \times \left(\frac{T}{1[\rm sec]} \right)^{\frac{1}{2}}
$$
$$
\times \left(\frac{x_{2\rm f}^{\rm rms}}{1.178 \times 10^{-16}[\rm m]} \right), \quad (26)
$$
$$
SNR_{3\rm f} = 73 \times \left(\frac{2.9 \times 10^{-20}[\rm m/\sqrt{Hz}]}{n_{48\rm Hz}} \right) \times \left(\frac{T}{1[\rm sec]} \right)^{\frac{1}{2}}
$$
$$
\times \left(\frac{x_{2\rm f}^{\rm rms}}{2.130 \times 10^{-18}[\rm m]} \right), \quad (27)
$$

where T is the integration time. If we integrate a signal larger than 3 min, we can measure $V_{2f}^{\rm R}$ and $V_{3f}^{\rm R}$ with sufficiently high SNR that systematic error can be reduced to less than 0.1 %.

This method used to measure the absolute laser power as well. The estimated powers are

$$
P_{2\rm f} = 0.023 \;[\rm W] \times \left(\frac{G}{6.6742 \times 10^{-11}[\rm m^3 kg^{-1} sec^{-2}]} \right)
$$
$$
\times \left(\frac{m_{\rm q}}{4.485[\rm kg]} \right) \times \left(\frac{r_{\rm q}}{0.200[\rm m]} \right)^2 \times \left(\frac{2[\rm m]}{d} \right)^4
$$
$$
\times \left(\frac{1}{\cos\theta} \right) \times \left(\frac{1}{1 + \frac{M}{I}\vec{a}\cdot\vec{b}} \right)^2, \quad (28)
$$
$$
P_{3\rm f} = 0.00095 \;[\rm W] \times \left(\frac{G}{6.6742 \times 10^{-11}[\rm m^3 kg^{-1} sec^{-2}]} \right)
$$
$$
\times \left(\frac{m_{\rm h}}{4.485[\rm kg]} \right) \times \left(\frac{r_{\rm h}}{0.125[\rm m]} \right)^3 \times \left(\frac{2[\rm m]}{d} \right)^5
$$
$$
\times \left(\frac{1}{\cos\theta} \right) \times \left(\frac{1}{1 + \frac{M}{I}\vec{a}\cdot\vec{b}} \right)^2. \quad (29)
$$

We estimate the laser power with following equations:

$$
\left(\frac{\delta P_{2\rm f}}{P_{2\rm f}} \right)^2 \sim 16\left(\frac{\delta V_{2\rm f}^{\rm R}}{V_{2\rm f}^{\rm R}} \right)^2 + 16\left(\frac{\delta V_{3\rm f}^{\rm R}}{V_{3\rm f}^{\rm R}} \right)^2 + \left(\frac{\delta P_{\rm sys}}{P_{\rm sys}} \right)^2, \quad (30)
$$
$$
\left(\frac{\delta P_{3\rm f}}{P_{3\rm f}} \right)^2 \sim 16\left(\frac{\delta V_{2\rm f}^{\rm R}}{V_{2\rm f}^{\rm R}} \right)^2 + 16\left(\frac{\delta V_{3\rm f}^{\rm R}}{V_{3\rm f}^{\rm R}} \right)^2 + \left(\frac{\delta P_{\rm sys}}{P_{\rm sys}} \right)^2, \quad (31)
$$

where $\delta P_{\rm sys}/P_{\rm sys}$ is the relative systematic error of the power due to the machining tolerance of the rotor masses

and radiuses, which are calculated by

$$\frac{\delta P_{\text{sys}}}{P_{\text{sys}}} \sim \frac{\delta G}{G} + \frac{\delta M}{M} + \frac{\delta \cos \theta}{\cos \theta} + \frac{\delta \left(1 + \frac{M}{I} \vec{a} \cdot \vec{b}\right)}{\left(1 + \frac{M}{I} \vec{a} \cdot \vec{b}\right)}$$
$$+ \frac{12}{\sqrt{6}} \frac{\delta r_{\text{h}}}{r_{\text{h}}} + \frac{10}{2} \frac{\delta r_{\text{q}}}{r_{\text{q}}} + \frac{5}{2} \frac{\delta m_{\text{q}}}{m_{\text{q}}} + \frac{4}{\sqrt{6}} \frac{\delta m_{\text{h}}}{m_{\text{h}}}. \quad (32)$$

We next consider the mitigating effect of the systematic error of the masses and radiuses due to the tolerance and uncertainty of the measurement instruments. The values of the masses and radiuses vary slightly with the tolerance of the fabrication process. The errors in m_{q}, r_{q}, m_{h}, and r_{h} are mitigated by the factor of $1/\sqrt{6}$ and $1/\sqrt{4}$. The uncertainty in the quadrupole and hexapole masses are limited by the accuracy of the electronic balance. In this case, we modeled masses made of Tungsten. The density of Tungsten is 19.25 g/cm^3. The diameter and thickness of the mass are 0.06 m and 0.08 m, respectively. Therefore, the mass of the rotor mass is 4.485 kg. We assumed that the CG-6000 electronic balance is used to weigh these means, with tolerance of 0.2 g [49]. Therefore, the relative uncertainty in the mass of the rotor mass is 0.004 %.

The rotor disk can be machined by Numerical Control milling. Dimensional accuracy of less than 0.02 mm can typically be achieved with this process. For measuring the shape, we assume that a three-dimension coordinate measuring machine (CMM) will be employed [50]. The precision of CMM is 2 μm. This indicates that we can measure the shape of the rotor and masses with sufficiently low uncertainty using the CMM.

The estimated relative uncertainties of the laser powers are 0.52 %. One of the largest uncertainties is the geometrical factor of the Pcal laser. The geometrical factor uncertainty is assumed to be 0.3 %, which is the same number as the instrument used in Advanced LIGO.

Finally, assuming that the statistical fluctuations of V_{in}, $s(\omega)$, $V_{2\text{f}}^{\text{R}}$, and $V_{3\text{f}}^{\text{R}}$ are independent for each measurement and therefore can be added in quadrature, the estimated relative uncertainty in the displacement measurements is written as

$$\left(\frac{\delta x}{x}\right)^2 \sim \left(\frac{\delta V_{in}}{V_{in}}\right)^2 + \left(\frac{\delta s(\omega)}{s(\omega)}\right)^2 + 25 \left(\frac{\delta V_{2\text{f}}^{\text{R}}}{V_{2\text{f}}^{\text{R}}}\right)^2 + 16 \left(\frac{\delta V_{3\text{f}}^{\text{R}}}{V_{3\text{f}}^{\text{R}}}\right)^2 + \left(\frac{\delta x_{\text{sys}}}{x_{\text{sys}}}\right)^2,$$
$$(33)$$

where $\delta x_{\text{sys}}/x_{\text{sys}}$ is the relative systematic error of the displacement which cannot be added in quadrature. This factor is written as

$$\frac{\delta x_{\text{sys}}}{x_{\text{sys}}} = \frac{\delta G}{G} + \frac{\delta M}{M} + \frac{12}{\sqrt{6}} \frac{\delta r_{\text{h}}}{r_{\text{h}}} + \frac{10}{2} \frac{\delta r_{\text{q}}}{r_{\text{q}}} + \frac{5}{2} \frac{\delta m_{\text{q}}}{m_{\text{q}}} + \frac{4}{\sqrt{6}} \frac{\delta m_{\text{h}}}{m_{\text{h}}}. \quad (34)$$

We assumed the mitigation factors of radiuses and masses discussed above in this calculation. To reduce the noise of the displacement measurement, we need to reduce the uncertainty in the shape of the rotor and masses. The uncertainties in $V_{2\text{f}}^{\text{R}}, V_{3\text{f}}^{\text{R}}, V_0^{\text{R}}$ are much less than that of other contributions. We can reduce the uncertainty of these values using long integration times with statistical measures. Each of the uncertainty is listed in Table II. The estimated total uncertainty of the displacement measurement is 0.17 %.

VI. CONCLUSION

Pcal are used in Advanced LIGO, Advanced Virgo and KAGRA. These devices are used to calibrate the interferometer response, and the uncertainty in the calibration affects the estimation of parameters of the GW source. In particular, the distance to the source strongly depends on the absolute laser power of the photon calibrator. In previous studies, the gold standard, in which the interferometer response is calibrated to the NIST laser power standard, was used for the absolute laser power calibration of the photon calibrator. However, the current standard for absolute laser power vary by a few % between different countries's metrology institutes. This uncertainty propagates directly to the calculation of the GW detector's absolute displacement. To address this problem, we proposed a combined calibration method that uses both a Pcal and a Gcal. The Gcal modulated the test mass using a dynamic gravity field. When canceling the displacement of the test mass using the Pcal, the Gcal was used to calibrate the interferometer responce.

This method had the advantage of offering a direct comparison between the amplitudes of the injected power and gravity field modulation at the test mass. Without the proposed gravity-field calibrator, the uncertainties of the optical efficiency through the window and mirrors and the geometrical factor of the laser position need to considered, because the working standard calibration is measured outside of the chamber. However, the method of gravity field can compare the displacement directly. Using this method, the uncertainty of the optical efficiency is avoided when calibrating the absolute laser power. The estimated laser power uncertainty with this method is 0.52 %. This result suggests that a new power calibration standard can be proposed that gains threefold improvement over the current standards.

Finally, we estimated the uncertainty of absolute calibration with the proposed method. The estimated absolute uncertainty in the displacement measurement is 0.17 %, which is a tenfold improvement on previous studies. This uncertainty affects the estimation of the distance to the gravitational wave source. This estimated uncertainty brings the precision of the Hubble constant to less than 1 %. This may address the tension between the Cephied-SN distance ladder [22] and CMB data assuming a ΛCDM model [23].

[1] B. P. Abbott *et al.* (LIGO Scientific Collaboration and Virgo Collaboration), Phys. Rev. Lett. **116**, 061102 (2016).
[2] J. Asai *et al.* (The LIGO Scientific Collaboration), Classical and Quantum Gravity **32**, 074001 (2015).
[3] F. Acernese *et al.*, Classical and Quantum Gravity **32**, 024001 (2015).
[4] K. Somiya, Classical and Quantum Gravity **29**, 124007 (2012).
[5] Y. Aso, Y. Michimura, K. Somiya, M. Ando, O. Miyakawa, T. Sekiguchi, D. Tatsumi, and H. Yamamoto (The KAGRA Collaboration), Phys. Rev. D **88**, 043007 (2013).
[6] B. P. Abbott *et al.* (LIGO Scientific Collaboration and Virgo Collaboration), Phys. Rev. D **93**, 122004 (2016).
[7] B. P. Abbott *et al.* (LIGO Scientific Collaboration and Virgo Collaboration), Phys. Rev. X **6**, 041015 (2016).
[8] C. Cahillane *et al.*, Phys. Rev. D **96**, 102001 (2017).
[9] B. P. Abbott *et al.* (LIGO Scientific and Virgo Collaborations), Phys. Rev. Lett. **116**, 221101 (2016).
[10] E. D. Hall, C. Cahillane, K. Izumi, R. J. E. Smith, and R. X. Adhikari, (2017), arXiv:1712.09719 [astro-ph.IM].
[11] B. P. Abbott *et al.*, The Astrophysical Journal **839**, 12 (2017).
[12] B. P. Abbott *et al.* (LIGO Scientific Collaboration and Virgo Collaboration), Phys. Rev. D **96**, 122004 (2017).
[13] K. Ono, K. Eda, and Y. Itoh, Phys. Rev. D **91**, 084032 (2015).
[14] K. Eda, K. Ono, and Y. Itoh, Journal of Physics: Conference Series **716**, 012026 (2016).
[15] B. P. Abbott *et al.*, The Astrophysical Journal Letters **833**, L1 (2016).
[16] B. P. Abbott *et al.* (LIGO Scientific Collaboration and Virgo Collaboration), Phys. Rev. Lett. **119**, 161101 (2017).
[17] B. P. Abbott *et al.* (LIGO Scientific, VINROUGE, Las Cumbres Observatory, DES, DLT40, Virgo, 1M2H, Dark Energy Camera GW-E, MASTER), Nature **551**, 85 (2017).
[18] B. F. Schutz, Nature **323**, 310 (1986).
[19] D. E. Holz and S. A. Hughes, The Astrophysical Journal **629**, 15 (2005).
[20] S. Nissanke *et al.*, The Astrophysical Journal **725**, 496 (2010).
[21] S. M. Feeney *et al.*, (2018), arXiv:1802.03404 [astro-ph.CO].
[22] A. G. Riess *et al.*, The Astrophysical Journal **826**, 56 (2016).
[23] P. A. R. Ade *et al.*, Astronomy and Astrophysics **594**, A13 (2016).
[24] D. Clubley *et al.*, Physics Letters A **283**, 85 (2001).
[25] K. Mossavi *et al.*, Physics Letters A **353**, 1 (2006).
[26] S. Karki *et al.*, Review of Scientific Instruments **87**, 114503 (2016).
[27] E. Goetz *et al.*, Classical and Quantum Gravity **27**, 084024 (2010).
[28] E. Goetz *et al.*, Classical and Quantum Gravity **26**, 245011 (2009).
[29] S. Kuck, EUROMET Comparison Project **156**, EUROMET.PR (2009).
[30] Figure. 9 at page 46. from [29] shows the absolute power measurement between the standard institute from nine countries. The systematic discrepancies between nine countries are as large as 3.5 %.
[31] R. L. Forward and L. R. Miller, Journal of Applied Physics **38**, 512 (1967).
[32] J. Sinsky and J. Weber, Phys. Rev. Lett. **18**, 795 (1967).
[33] J. A. Sinsky, Phys. Rev. **167**, 1145 (1968).
[34] H.Hirakawa, K.Tsubono, and K.Oide, Nature **283** (1980).
[35] K. Oide, K. Tsubono, and H. Hirakawa, Japanese Journal of Applied Physics **19**, L123 (1980).
[36] T. Suzuki *et al.*, Japanese Journal of Applied Physics **20**, L498 (1981).
[37] Y. Ogawa, K. Tsubono, and H. Hirakawa, Phys. Rev. D **26**, 729 (1982).
[38] K. Kuroda and H. Hirakawa, Phys. Rev. D **32**, 342 (1985).
[39] P. Astone *et al.*, Zeitschrift für Physik C Particles and Fields **50**, 21 (1991).
[40] P. Astone *et al.*, The European Physical Journal C - Particles and Fields **5**, 651 (1998).
[41] L. Matone *et al.*, Classical and Quantum Gravity **24**, 2217 (2007).
[42] P. Raffai, G. Szeifert, L. Matone, Y. Aso, I. Bartos, Z. Márka, F. Ricci, and S. Márka, Phys. Rev. D **84**, 082002 (2011).
[43] D. Tuyenbayev *et al.*, Classical and Quantum Gravity **34**, 015002 (2017).
[44] Y. Inoue *et al.*, In preparation (2018).
[45] B. N. Taylor and C. E. Kuyatt, *Guidelines for Evaluating and Expressing the Uncertainty of NIST Measurement Results*, Tech. Rep. (NIST Tecnical Note 1297, 1994).
[46] P. J. Mohr, D. B. Newell, and B. N. Taylor, Rev. Mod. Phys. **88**, 035009 (2016).
[47] Y. Michimura *et al.*, Classical and Quantum Gravity **34**, 225001 (2017).
[48] SUMCON, https://gwdoc.icrr.u-tokyo.ac.jp/cgi-bin/DocDB/ShowDocument?docid=3729.
[49] CG-6000, http://www.vibra.co.jp.
[50] Y. Inoue *et al.*, Appl. Opt. **55**, D22 (2016).